Inhibition of Localized Corrosion Propagation on Carbon Steel: A Potentiostatic Study

Bernardo Augusto Farah Santos,[‡,]* Maria Eduarda Dias Serenario,* Xi Wang,* David Young,* Marc Singer,* Maalek Mohamed-Saïd,** Shuai Ren,* Yi He,* and Alysson Helton Santos Bueno***

The occurrence of localized corrosion in carbon steel pipelines, even when the uniform corrosion rate remains low, is a major concern in the hydrocarbon production and transmission industry. The propagation of these pits, caused by the galvanic coupling between the inhibited surface and the active pit, can lead to serious consequences such as financial loss, environmental damage, production interruption, and even loss of life. To better understand this phenomenon, this work focuses on using the potentiostatic technique to evaluate the tendency of localized corrosion propagation. The experiments were conducted using a primarily imidazolinium-based corrosion inhibitor in produced water conditions (5 wt% NaCl, pH 4.5, CO_2-saturated) at 55°C and 80°C. The baseline results were obtained through linear polarization resistance and potentiodynamic polarization tests. The potentiostatic experiments were then conducted to artificially simulate different levels of galvanic coupling that could exist in case of active localized corrosion. The results showed that, at certain anodic potentials, increased inhibitor dosage was necessary to significantly decrease the current. However, at high current levels, further injections were insufficient, indicating that substrate dissolution may affect the adsorption of the inhibitor. This work provides insights into the role of inhibitors and important factors in stopping the propagation of localized corrosion of carbon steel. Further research, such as designing a proper zero-resistance ammeter setup, will be necessary to fully understand this complex phenomenon. The results show that the potentiostatic methodology can be a rapid and easy alternative to obtain electrochemical information and improve understanding of localized corrosion propagation.

KEY WORDS: corrosion inhibition, high temperature, imidazoline, inhibition efficiency, localized corrosion propagation, potentiostatic

INTRODUCTION

The transportation of petroleum and related products over long distances in the oil and gas industry typically occurs via large-diameter carbon steel pipelines.[1-2] Localized corrosion is known as the most dangerous and unpredictable corrosion mechanism found in hydrocarbon production and transmission systems. This mode of corrosion has the potential to cause serious financial loss, environmental damage, production interruption, and even loss of life. Over the years, corrosion engineers have made significant improvements in prediction and mitigation techniques to extend the lifespan of carbon steel pipelines, such as using corrosion inhibitors (CIs);[3-5] injection of such chemicals has proven to be effective and economical, making them a first choice over other alternatives. However, the long-term use of organic CIs in the oil and gas industry has shown a high potential for the occurrence of localized attacks.[6] This might take place when the inhibitor is not appropriate to the operating conditions or when the inhibitor dosage is too low, in the presence of corrosion product layers or sand, or when the pipeline surface is exposed to extreme shear stress.[6-7] Although pit initiation has been widely reported in the presence of inhibitors,[6,8-9] discussion of propagation has been limited.

The propagation process is typically driven by the local galvanic coupling established between the area covered by the corrosion products or CIs and the bare steel surface area of the pit. Galvanic current drives the propagation of the pit causing severe damage to exposed metal surfaces. Some authors[10-12] attempted to simulate this mechanism using cells composed of two electrodes—a cathode and an anode—in which they had their surface properly prepared to act as such and then were connected via a zero-resistance ammeter (ZRA) to monitor the galvanic current. The separation between the electrodes giving rise to ohmic resistance was one of the challenges faced by the authors.[12] The poor understanding of the involved phenomena stems from the complex system that does not lend itself to artificial simulation. Thus, it is important to develop methodologies that aim to simulate the mechanisms involved.

While the ZRA setup mentioned above is the "gold standard" when investigating galvanic coupling, other, less complicated, techniques can be used to give some insights into the phenomena. The potentiostatic methodology emerges as an interesting rapid and easy alternative to simulate artificially such a localized phenomenon using only one working electrode in a conventional three-electrode electrochemical cell. Once a potential is applied to the working electrode,

Table 1. *Composition (wt%) of Flat C1018 Carbon Steel Specimens*

Element	C	Al	Cu	Mn	Mo	Ni	S	Si	Fe
Composition	0.16	0.007	0.088	0.65	0.019	0.055	0.010	0.25	Balance

a current will be induced. Such a current simulates the dissolution of an actively corroding pit. One should be able to apply different ranges of potential to the artificial anode simulating the propagation of localized corrosion that might take place following the aforementioned model. Therefore, if the inhibitor is efficient, one should observe a decrease in the current flowing through the sample when injecting the CI into the solution. The methodology would also allow a better understanding of the electrochemical parameters that govern the adsorption/desorption mechanisms of the inhibitors as well as improve the existing models[13] for this matter. Consequently, the objective of this work is to utilize the potentiostatic methodology to further understand the role of inhibitors and important factors in stifling the propagation of localized corrosion of carbon steel. The next step of this work will be to design a proper ZRA setup and repeat this study.
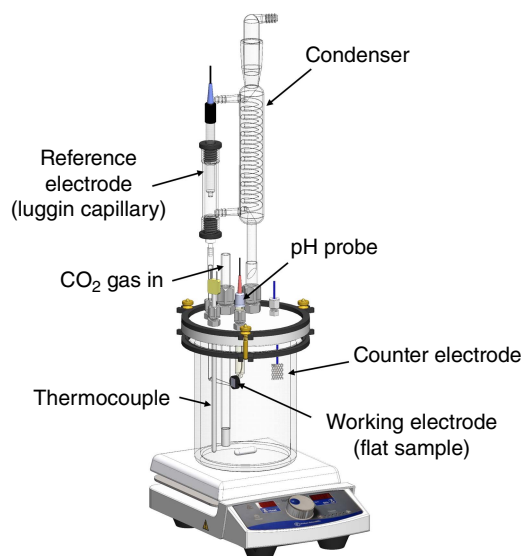
EXPERIMENTAL PROCEDURES

2.1 | Materials and Chemicals

Carbon steel C1018 (UNS G1018[(1)]) was machined into flat and squared specimens with a surface area of ca. 1.6 cm^2 and mounted in epoxy for the electrochemical experiments. The chemical composition of the material used was listed in Table 1. The ferritic and pearlitic microstructure contained 2.28 wt% of cementite phase (Fe_3C) according to the lever rule.[14] The surface was ground with #180 and #400 grit silicon carbide abrasive paper with water flow, finished with #600 grit SiC abrasive paper with isopropanol flow, cleaned in an ultrasonic isopropanol bath, and air-dried prior to each experiment.

All experiments were performed using a 2 L glass cell as depicted in Figure 1. Only one C1018 epoxy-mounted sample was used in each test. The electrolyte was an aqueous solution with 5 wt% NaCl, CO_2 as sparging gas, 1 bar total pressure, and pH 4.5. Temperatures of 55°C and 80°C were assessed. Prior to each experiment, the electrolyte was sparged with CO_2 for at least 2 h to deoxygenate; sparging was continuous during each experiment to avoid any oxygen ingress and maintain CO_2 saturation. The pH of the solution was maintained at 4.5±0.1 by adding hydrochloric acid (HCl) and sodium bicarbonate ($NaHCO_3$). The CI used in this study is an imidazolinium-based commercial inhibitor in a concentration of 50 ppm. This dosage is recommended by the manufacturer and it is above the surface saturation concentration (SSC)[15] for both temperatures studied here.

2.2 | Electrochemical Measurements

A three-electrode electrochemical cell was used having a Pt-coated mesh as the counter electrode, a KCl-saturated Ag/AgCl reference electrode (connected to the glass cell via a salt bridge and a Luggin capillary), and the C1018 as the working electrode. The electrochemical measurements were conducted using a Gamry PCI4G300-42065 potentiostat. Open-circuit potential (OCP), electrochemical impedance

FIGURE 1. *2 L glass cell setup.*

spectroscopy (EIS), and linear polarization resistance (LPR) measurements were taken. The EIS data were collected at OCP from 5 kHz to 1 Hz with a perturbation amplitude of 10 mV rms. The LPR measurements were conducted using a range from −5 mV_{OCP} to +5 mV_{OCP}, with a scan rate of 0.125 mV/s using a B value of 26 mV[16-17] for corrosion rate calculations. At the conclusion of each experiment, a cathodic potentiodynamic sweep was conducted. The anodic potentiodynamic sweep was conducted after the OCP returned to the original value before the cathodic sweep.

2.3 | Baseline Experiments

Establishing baselines of uninhibited and fully inhibited bare steel prior to the potentiostatic experiments is essential to understand the potential and current density ranges in which the material will respond whenever a potential is applied. In this step, the corrosion rates were monitored using LPR for 5 h under inhibited and uninhibited conditions. For the inhibited environment, the inhibitor was injected into the solution after 20 min of precorrosion. For both conditions, after assessing the corrosion rate evolution, potentiodynamic sweeps took place cathodically and anodically.

2.4 | Potentiostatic Experiments

At this stage, before applying any potential to the sample, the sample stayed in the solution for OCP stabilization for 20 min. The working electrode was then polarized to four different positive fixed potentials over the OCP of the bare steel ($mV_{OCP, bare steel}$), simulating possible scenarios:

- +25 $mV_{OCP, bare steel}$—to simulate the localized corrosion propagation when there is a galvanic coupling established between a surface covered with iron carbonate ($FeCO_3$) and the active surface of the pit (bare surface).[11]

- +70 mV$_{OCP, bare steel}$—to simulate the localized corrosion propagation when there is a more severe galvanic coupling established between the surface covered with CIs and the active surface of the pit.
- +100 mV$_{OCP, bare steel}$—to simulate a more extreme condition in which the difference in potential is higher than the OCP difference between the area covered and the area uncovered with inhibitor.
- +150 mV$_{OCP, bare steel}$—to apply an over potential in the sample close to the desorption potential[18] observed in the baseline tests.

For all potentiostatic tests, the potential was applied to the sample in an uninhibited environment (5 wt% NaCl, pH 4.5, CO_2) for 300 s (5 min), and then 50 ppm of the CI was injected into the solution. The induced current was monitored throughout the experiment, and an additional dosage of the inhibitor was added when necessary.

RESULTS AND DISCUSSION

3.1 | Baseline Experiments

The change in corrosion rate (from LPR) over time is shown in Figure 2 for both inhibited (CI) and bare steel environments at 55°C and 80°C. Bare steel conditions show no significant change, with slightly higher corrosion rates of around 3 mm/y after 5 h at 80°C. Injection of the CI greatly reduces the corrosion rates for both temperatures, with values as low as 0.1 mm/y after 5 h at 55°C. However, it is important to note that 80°C still had a residual corrosion rate above 0.1 mm/y after 5 h.

The main objective of this section is to record the anticipated anodic current during potentiostatic tests. Figure 3 displays the anodic potentiodynamic sweeps that were conducted in the four conditions (55°C and 80°C with/without inhibitor).

The anodic sweeps in the uninhibited environment at both temperatures were similar, with the one at 55°C slightly retarded to the one at 80°C. Temperature also played a negative role in the inhibited environment as the curve associated with 80°C was slightly accelerated in relation to that observed at 55°C. A significant observation was the "desorption point" for the anodic sweep in the inhibited condition. The literature suggests that when the potential exceeds a certain critical anodic
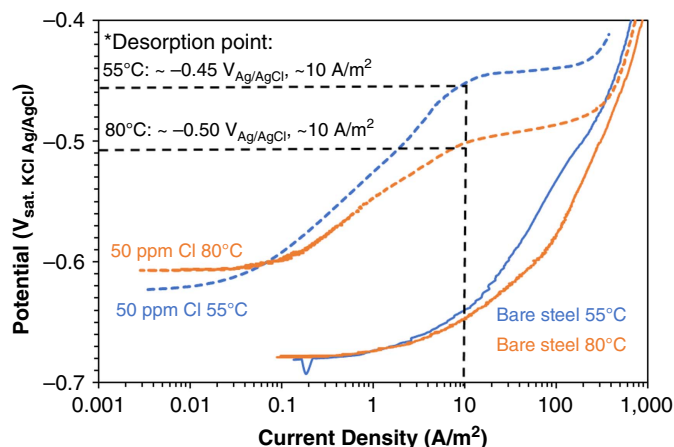

FIGURE 3. Baseline anodic sweeps for the inhibited and uninhibited conditions at 55°C and 80°C.

potential, the inhibitor adsorbed on the steel surface may be fully or partially desorbed. This has been previously reported in the literature by Drazic and Drazic[19] in their adapted equation for the Langmuir isothermal model. In their work, aside from the natural adsorption and desorption components of the equation, they suggest that in reactive surfaces there is a third component regarding the electrochemical desorption of the inhibitor molecules there is dependent on the current density that flows onto the metal surface. A more realistic Langmuir adsorption model was proposed as follows:

$$\frac{d\theta}{dt} = \overrightarrow{r} - \overleftarrow{r_1} - \overleftarrow{r_2} = \overrightarrow{k_a(1-\theta)c} - \overleftarrow{k_d\theta} - \overleftarrow{k_3j\theta} \tag{1}$$

where $\overrightarrow{r}$ and $\overleftarrow{r_1}$ are the natural adsorption and desorption component, respectively, and $\overleftarrow{r_2}$ is the electrochemical desorption component. When reached equilibrium, $d\theta/dt = 0$:

$$\theta = \frac{k_a c}{k_a c + k_d + k_3 j} \tag{2}$$

where k_3 is considered the rate constant for the electrochemical desorption reaction (unitless) and j is the corrosion
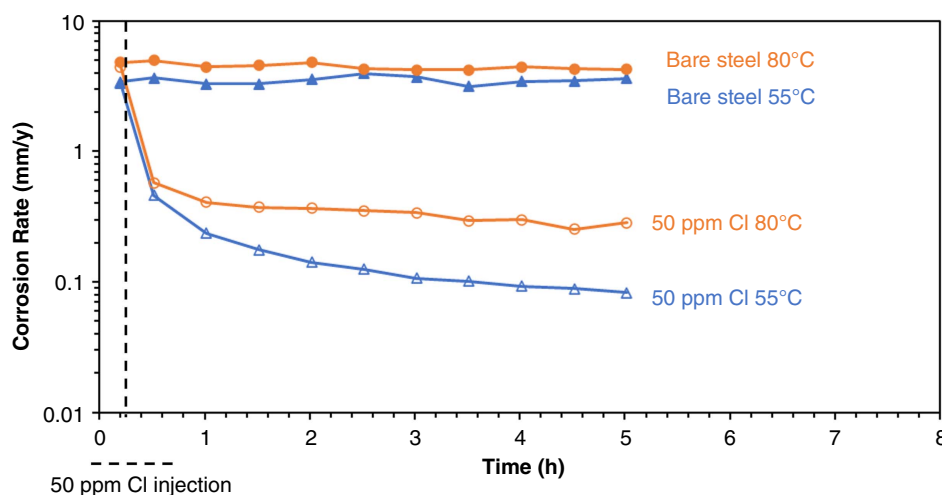

FIGURE 2. LPR corrosion rates over time for the inhibited and uninhibited conditions at 55°C and 80°C.

current density. Therefore, the desorption point can be assumed to be the threshold at which the inhibitor molecule adsorption to the surface is unaffected. Although there was a significant difference in potential for the desorption point for each temperature, the value observed for the current density was similar. That upholds the assumption made by Drazic and Drazic that the current density is the main parameter for electrochemical desorption. Thus, it is possible to suggest that full inhibitor adsorption is unlikely to occur for a sample polarized with a current density higher than the one registered for the desorption point.

3.2 | Potentiostatic Experiments

Hereinafter, the approach is to compare the current response before and after the addition of the inhibitor to the polarized sample. This comparison should provide insights into whether the injection of the inhibitor can suppress high-anodic currents caused by polarization, simulating the behavior of an anodic site on steel subjected to galvanic coupling with the addition of the inhibitor.

3.2.1 | +25 mV$_{OCP, bare steel}$

Figure 4 displays anodic polarization scans that indicate the range of current densities (e.g., around 5 A/m^2 at 55°C for bare steel) expected when applying +25 mV$_{OCP, bare steel}$. With the addition of the corrosion inhibitor, the current density should shift from the values for bare steel (left plot) to the values shown for the inhibited anodic sweep (right plot). As indicated in the figure, with the fixed potential, negative currents should be observed after the injection of the inhibitor, as the fixed potential falls on the cathodic side of the inhibited baseline potentiodynamic sweep.

Figure 5 displays the current densities during the +25 mV$_{OCP, bare steel}$ potentiostatic experiment at 55°C and 80°C. During the initial 300 s, with no inhibitor present, the current densities were stable, though they slightly decreased at 80°C before the CI was added. Upon injection of the inhibitor, the current dropped significantly for both temperatures, reaching negative values in less than 200 s, as indicated by the baseline curves in Figure 3. After 2,000 s, both currents stabilized at a negative level, indicating full adsorption of the inhibitor, and the measured currents were consistent with the baseline tests.

The inhibitor adsorption resulted in a greater increase in the corrosion potential of bare steel compared to the applied potential (intrinsic potential difference due to surface condition difference). In a real-world scenario, this led to a role reversal, where the previously corroding "anode" now acted as the cathode, promoting the cathodic reaction and slowing down the anodic dissolution. As a result, the measured net current was negative, indicating the dominance of the cathodic reaction. Although this is unlikely to happen in situ, once one should observe inhibitor adsorption both in the anode and in the cathode of a real galvanic coupling, the result enlightens about the limitations of the technique when addressing the effects on the cathode, though it is still useful for academic purposes. To avoid the occurrence of a role reversal in this scenario, the use of the galvanostatic current should be implemented instead, applying a fixed current and observing the shift in potential.

3.2.2 | +70 mV$_{OCP, bare steel}$

The baseline current densities for the +70 mV$_{OCP, bare steel}$ potentiostatic experiment can be seen in Figure 6. This scenario aimed to simulate the propagation of localized corrosion when the substrate lacked inhibitor coverage. As shown in Figure 7, the
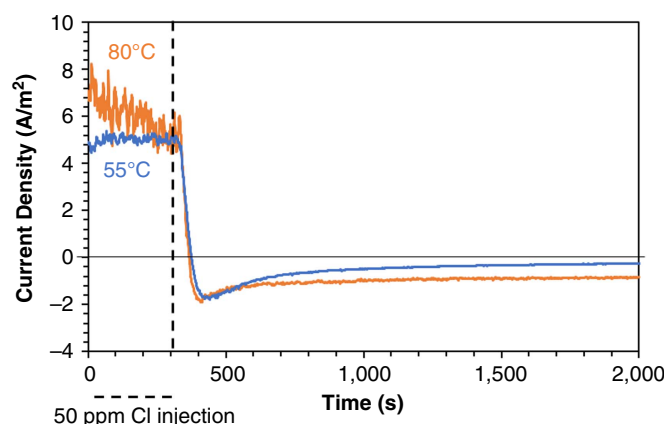

FIGURE 5. *Net current density over time for +25 mV$_{OCP, bare steel}$ potentiostatic experiment. Condition: 5 wt% NaCl, CO$_2$, pH 4.5, 50 ppm Cl added after 300 s.*
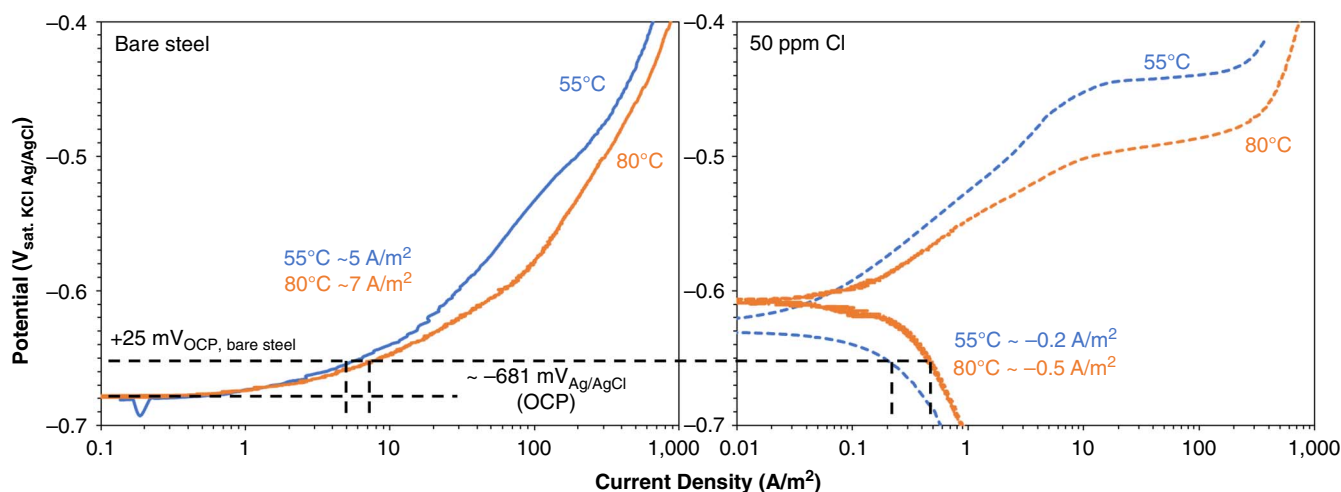

FIGURE 4. *Anodic polarization curves showing the current density expected for bare steel (left) and inhibited environment (right) during +25 mV$_{OCP, bare steel}$ potentiostatic experiment. Condition: 5 wt% NaCl, CO$_2$, pH 4.5, 50 ppm Cl.*
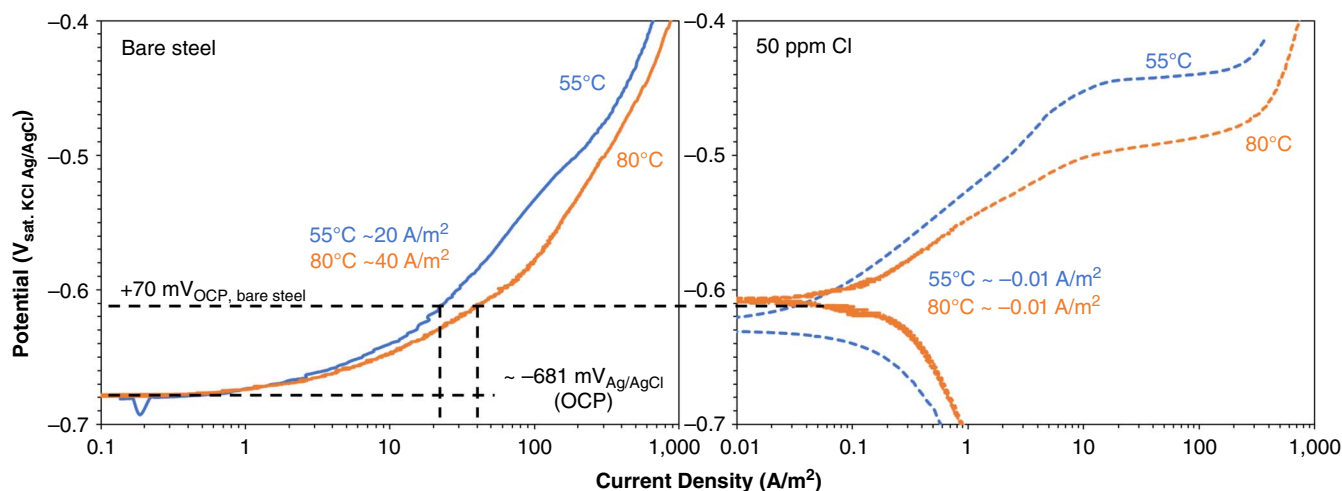
FIGURE 6. *Anodic polarization curves showing current density expected for bare steel (left) and inhibited environment (right) during +70 mV*$_{OCP, bare steel}$ *potentiostatic experiment. Condition: 5 wt% NaCl, CO$_2$, pH 4.5, 50 ppm Cl.*

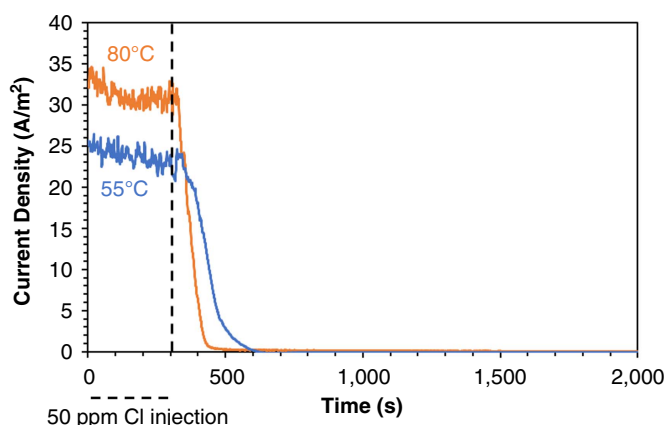**FIGURE 7.** *Net current density over time for +70 mV*$_{OCP, bare steel}$ *potentiostatic experiment. Condition: 5 wt% NaCl, CO$_2$, pH 4.5, 50 ppm Cl added after 300 s.*

applied potential is near the measured OCP in the inhibited environment (Figure 5), so the current densities should reach a stable value of around 0 A/m^2 for both temperatures.

Figure 7 shows that the initial current densities, if translated to corrosion rates, were higher at higher temperatures during the first 300 s of the uninhibited period, at 26.9 mm/y and 36.1 mm/y for 55°C and 80°C, respectively. After the inhibitor was added, the current densities decreased, stabilizing at a low level that was similar to the levels shown in Figure 6's baseline curves. This implies that the applied potential was not strong enough to prevent the inhibitor's adsorption on the specimen surface, meaning that substrate dissolution did not affect the adsorption of the inhibitor molecules. These results contradict what is expected when considering the desorption point theory aforementioned. The current densities prior to inhibitor addition were higher than the value observed for both temperatures in Figure 3. Thus, one should not expect a significant decrease in current when the inhibitor was added once the electrochemical desorption rate should undermine the adsorption. It suggests that the potential recorded at the desorption point must be considered, and not only the current as addressed by Drazic and Drazic.[19] Some authors reported the increase in

inhibition efficiency by observing the shift in the desorption potential to more positive values,[20] though nothing about the dependence on the current density is mentioned. Others reinforce the role of the potential on promoting the electrostatic repulsion that would weaken the adsorption bond between the inhibitor and metal surface.[21] The next potentiostatic results will give a better understanding of the potential effect on the adsorption kinetics.

3.2.3 | +100 mV$_{OCP, bare steel}$

Figure 8 displays the anticipated baseline current densities in the +100 mV$_{OCP, bare steel}$ potentiostatic experiment. Despite the applied potential being higher than the OCPs in the inhibited environment, the resulting inhibited current densities should still be noticeably lower than the uninhibited condition.

Figure 9 depicts a decrease in current density at both temperatures following the inhibitor injection. However, instead of leveling off at a very low value, around 0.1 A/m^2 to 0.2 A/m^2, as shown in Figure 8, the current densities rose and stabilized at higher levels (7.2 A/m^2 at 55°C and 26.4 A/m^2 at 80°C). The range between the OCP of the inhibited condition and the desorption potential appears to create an unstable region for the inhibitor on the surface. Although the inhibitor initially adheres to the surface, the high-current density from substrate dissolution overpowers it, causing a lack of full coverage. The higher the potential difference from the uninhibited state, the more difficult it becomes for the inhibitor to adhere and prevent substrate dissolution.

Stabilized at high values, extra injections of the corrosion inhibitor were conducted to see if further inhibition could occur (as shown in Figure 10). The subsequent drop in current after the second injection shows a clear dependence on the dosage for inhibiting a polarized surface. This may be due to the depletion of bulk Cl concentration in a closed system, requiring extra doses. However, even after 15,000 s (around 4 h) at higher temperatures, current densities remained high (about 2.91 A/m^2). The tests showed that corrosion rates were 0.05 mm/y at 55°C and 3.13 mm/y at 80°C, as calculated from current densities using the equation from ASTM-G102.[22]

Although the concentration of 50 ppm is already above the inhibitor SSC, it is important to highlight that SSC calculations are conducted in ideal conditions,[15] when the sample corrodes
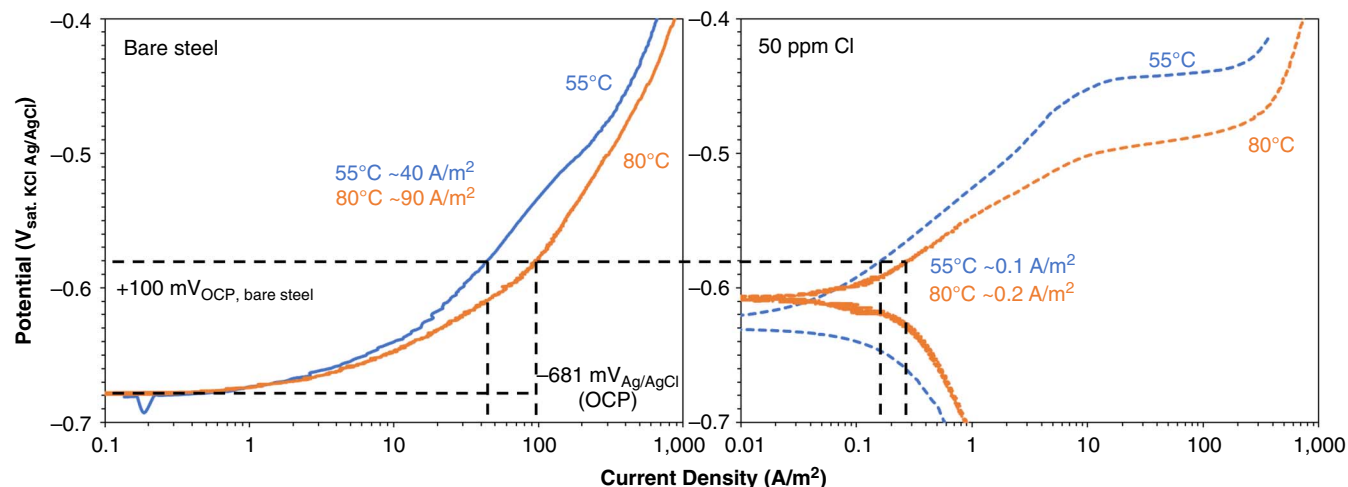
FIGURE 8. *Anodic polarization curves showing current density expected for bare steel (left) and inhibited environment (right) during +100 mV$_{OCP, bare steel}$ potentiostatic experiment. Condition: 5 wt% NaCl, CO$_2$, pH 4.5, 50 ppm Cl.*

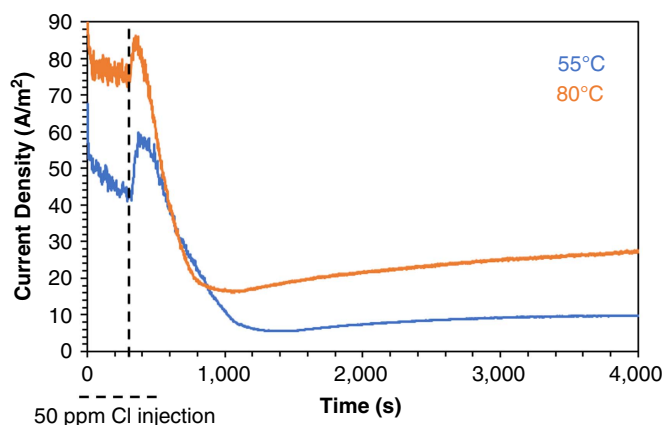**FIGURE 9.** *Net current density over time for +100 mV$_{OCP, bare steel}$ potentiostatic experiment. Condition: 5 wt% NaCl, CO$_2$, pH 4.5, 50 ppm Cl added after 300 s.*
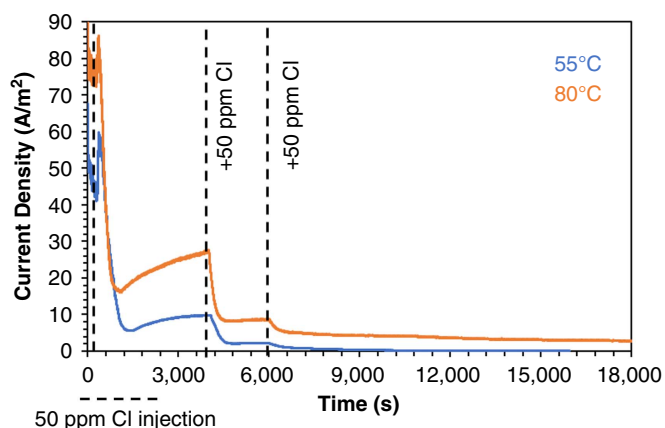

FIGURE 10. *Continuation of the +100 mV$_{OCP, bare steel}$ potentiostatic experiment. Condition: 5 wt% NaCl, CO$_2$, pH 4.5, with two additional dosages of 50 ppm Cl added at different times.*

at its OCP, i.e., low-current density. However, when there is a current flowing with a significant magnitude, the local inhibitor depletion observed near the surface is not considered during

SSC calculations. Therefore, it is plausible to expect that under more critical scenarios a higher dosage of the inhibitor will be necessary to provide the same efficiency as the one observed during baseline tests.

3.2.4 | +150 mV$_{OCP, bare steel}$

Figure 11 displays anodic polarization scans, revealing the anticipated range of current densities for the experiment at +150 mV$_{OCP, bare steel}$. Despite being closer to the desorption potential indicated by the polarization curves, if the inhibitor is effective, the current density should decrease by at least two orders of magnitude as shown by the baseline polarization curve.

Figure 12 reveals that after injecting the corrosion inhibitor, the current densities increased compared to the initial 300 s in the uninhibited environment. In the instability potential range, it can be assumed that as the desorption potential is approached, it becomes more difficult for the inhibitor to adsorb on the polarized surface due to increased iron dissolution.

An additional inhibitor dosage was added to the solution for both temperatures after the corrosion rates stabilized. At 80°C, despite a temporary decrease in current density after each injection, it quickly started increasing again, suggesting that the substrate's dissolution was likely hindering the inhibitor's ability to adsorb on the surface, regardless of the concentration of the inhibitor in the solution. At this point, it is possible to state that the magnitude of the current density flowing on the metal surface was decisive in impeding inhibitor adsorption. Table 2 summarizes the main findings of this work.

Corrosion rates were calculated from the equation at ASTM G102,[22] using Rp values for the baseline and steady-state current density (j) for the potentiostatic tests. CR$_0$ stands for the corrosion rates under an uninhibited environment, CR$_{i, 50 ppm}$ the rate under an inhibited environment with 50 ppm of inhibitor, and CR$_{i, 150 ppm}$ when the inhibitor concentration was tripled. Inhibitor efficiency (IE) was calculated according to the following equation:[23-24]
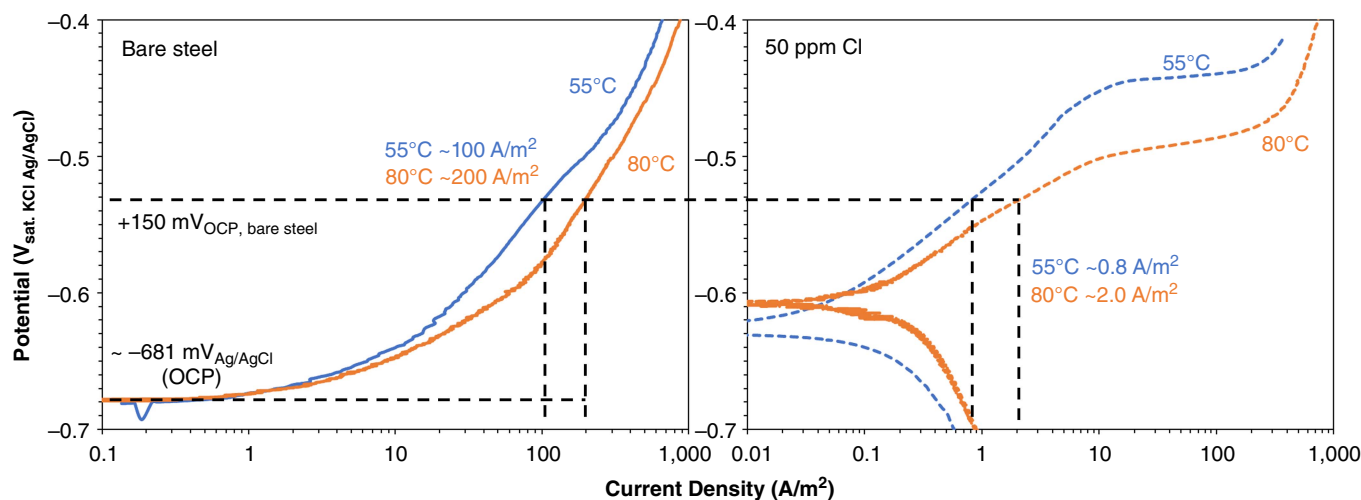
$$IE(\%) = \frac{CR_0 - CR_i}{CR_0} \times 100 \qquad (3)$$

FIGURE 11. *Anodic polarization curves showing current density expected for bare steel (left) and inhibited environment (right) during +150 mV$_{OCP, \text{ bare steel}}$ potentiostatic experiment. Condition: 5 wt% NaCl, CO$_2$, pH 4.5, 50 ppm Cl.*

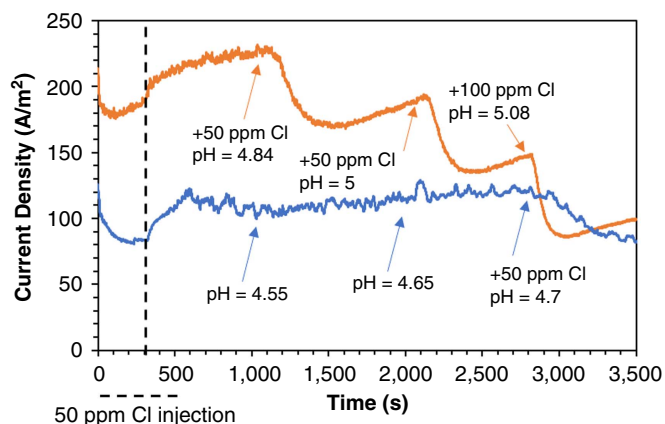**FIGURE 12.** *Net current density over time for +150 mV$_{OCP, \text{ bare steel}}$ potentiostatic experiment. Condition: 5 wt% NaCl, CO$_2$, pH 4.5, and several dosages of Cl were added at different times.*

The calculated values shown are the average considering all repetitions, and the maximum and minimum obtained are displayed. Inhibitor efficiency was also calculated for the additional dosage of the inhibitor to highlight the effect of increasing its concentration. For the conditions with negative values after inhibitor injection or with an increase in the initial current density, IE was not calculated. As expected, IE for the baseline at 80°C was lower than at 55°C, though more than 90% was reached. Concerning condition +70 mV$_{OCP, \text{ bare steel}}$, the efficiency calculated from the stabilized current density values observed before and after the inhibitor injection indicated a higher efficiency than the observed for the baseline, at both 55°C and 80°C experiments. It is important to highlight that the main reason for such a high efficiency lies in the fact that the initial current density values during the uninhibited value were extremely high. For the +100 mV$_{OCP, \text{ bare steel}}$ condition, 50 ppm of inhibitor resulted in only 80.82% and 64.28% for 55°C and 80°C, respectively. The numbers clearly indicate a lack of inhibition under these scenarios, which was improved with the increase of inhibitor concentration to 150 ppm (two extra doses of 50 ppm), leading to IE equal to 99.93% at 55°C and 96.22% at 80°C.

Regarding the critical conditions (+100 mV$_{OCP, \text{ bare steel}}$, and +150 mV$_{OCP, \text{ bare steel}}$), Figures 9 and 12 show a significant discrepancy between the current density measured and the one expected from the respective baselines. Before elucidating the reason why the inhibitor failed at potentials close to but still lower than the "desorption potential," it is important to highlight that the high amount of cementite (2.28%) presented in the C1018 microstructure can play a significant role in hindering the inhibition. In such microstructure, the ferrite tends to be consumed preferentially over the cementite.[2,25] Therefore, as the material corrodes, the cementite network will be revealed on the surface, increasing the material exposed area. The thicker the cementite layer is, the more unlikely it is to observe a good inhibition, because there will be an increase in the cathodic kinetics due to the increased cathodic area.[26-27] Thus, in this present work, a higher applied potential leads to a thicker cementite layer due to the fast dissolution of ferrite. The thicker cementite layer in turn supported faster cathodic kinetics, and hence the inhibition will be lost at high potentials. Calculation of the metal thickness loss through Faraday's law estimated ca. 23 μm and ca. 40 μm at 55°C and 80°C, respectively. It suggests the existence of a cementite matrix being exposed on the surface and being thick enough to impede the adsorption process of the inhibitor on the anodically polarized phase (ferrite).

Although some authors have reported the negative effects played by the changes on the metal surface characteristics, i.e., the presence of corrosion products or microstructure phase networks,[27-29] little has been discussed about the inhibition of an actively corroding surface. Once it is understood that the surface conditions will be different for inhibitor adsorption during potentiostatic experiments over the baseline ones, an adjusted potentiodynamic sweep was plotted to consider the parameters of each experiment and compare them with the baseline sweeps. The methodology developed was as follows:

- Various fixed current densities (galvanostatic mode—to guarantee the current flux in one direction only) were

Table 2. *Summary of Results Obtained*

Condition	55°C					80°C				
	CR$_0$ (mm/y)	CR$_{i,\ 50\ ppm}$ (mm/y)	IE (%)	CR$_{i,\ 150\ ppm}$	IE 150 ppm (%)	CR$_0$ (mm/y)	CR$_{i,\ 50\ ppm}$ (mm/y)	IE (%)	CR$_{i,\ 150\ ppm}$	IE 150 ppm (%)
Baseline	3.67±0.19	0.09±0.02	97.63±0.01	–	–	4.26±0.02	0.34±0.09	91.85±2.24	–	–
+25 mV$_{OCP,\ bare\ steel}$	5.98±0.18	–	–	–	–	6.78±0.62	–	–	–	–
+70 mV$_{OCP,\ bare\ steel}$	31.63±3.97	0.07±0.01	99.76±0.02	–	–	36.76±0.97	0.014±0.002	99.96±0.01	–	–
+100 mV$_{OCP,\ bare\ steel}$	53.77±1.11	10.32±0.97	80.82±1.41	0.03±0.01	99.93±0.03	84.45±0.02	30.16±0.62	64.28±0.73	3.19±0.17	96.22±0.21
+150 mV$_{OCP,\ bare\ steel}$	106±4	143±2	–	–	–	187±17	340±89	–	–	–

selected to be applied to the sample using the same aforementioned procedure (50 ppm of inhibitor injected after 300 s).

- When the response in potential reached a steady-state value, the value was recorded for each condition and used to plot an adjusted anodic sweep for the inhibitor under the polarizing condition.

Figure 13 shows the comparison between the baseline curves and the adjusted one. Emphasis should be placed on the fact that the adjusted curve is composed of the union of multiple points and was not derived using conventional methods.

The adjusted anodic sweep exhibits greatly accelerated kinetics compared to the baseline curve inhibited with 50 ppm CI on a newly polished surface. However, this inhibition effect should not be anticipated on sites of localized corrosion propagation. For instance, the +150 mV$_{OCP,\ bare\ steel}$ lies in a region (as shown in Figure 13) where the material has already started to behave like bare steel, implying that inhibitor adsorption on the surface has been suppressed. As a result, the current density values for +100 mV$_{OCP,\ bare\ steel}$ are now more similar to those observed earlier in Figure 9.

It is important to note that this approach is very seminal and other electrochemical factors, which have received less attention in the work, may be contributing to the inhibitor's failure under these conditions. Although adjusting the curve is not the most effective means of determining the trend, it provides insight into how the cementite network and the polarized surface are negatively impacting the inhibition. The following issues, which may have arisen from experimental artifacts, require further investigation:

- The CI concentration in the bulk may have been depleted due to the tests being performed in a closed system with a single CI injection.
- The efficacy of other commercial CIs in limiting localized corrosion propagation should be tested, as it depends on the type of CI.
- All tests were conducted with artificially imposed currents to simulate localized corrosion propagation configuration. Ongoing work aims to recreate the same configuration with a real galvanic setup and varying anode/cathode surface ratios.
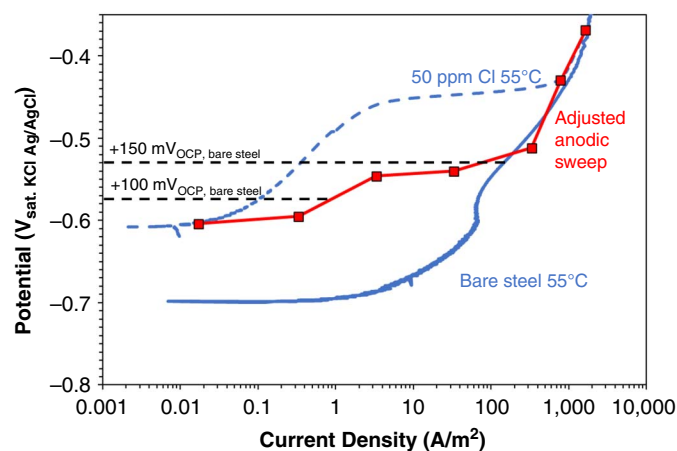

FIGURE 13. *Adjusted anodic sweep for inhibited environment considering the sample being polarized. Condition: 5 wt% NaCl, CO$_2$, pH 4.5, 55°C, 50 ppm CI.*

CONCLUSIONS

This work presents a new approach to evaluate inhibition regarding localized corrosion propagation on carbon steel, under exploration-produced water conditions (5 wt% NaCl, pH 4.5, CO_2, 55°C to 80°C). The following conclusions can be drawn from the above results:

➢ The capacity of the CI to adhere to the polarized sample is contingent on the magnitude of the current density flowing on the sample surface.

➢ At over potentials near the desorption potential in the inhibited solution, additional amounts of CI are required to suppress the anodic dissolution and reduce the net current density to values comparable to those seen in the baseline experiments.

➢ The methodology focuses solely on the effects of the inhibitor on the anode in a simulated galvanic coupling. The effects on the cathode that result from the injection of the inhibitor could also be studied by using a real galvanic coupling setup with two electrodes serving as anode and cathode.

ACKNOWLEDGMENTS

References

1. B.A.F. Santos, R.C. Souza, M.E.D. Serenario, M.C. Gonçalves, E.P. Mendes Júnior, T.A. Simões, J.R. Oliveira, G.L. Vaz, L. Caldeira, J.A.C.P. Gomes, A.H.S. Bueno, *J. Nat. Gas Sci. Eng.* 80 (2020): p. 103405.
2. B.A.F. Santos, M.E.D. Serenario, R.C. Souza, J.R. Oliveira, G.L. Vaz, J.A.C.P. Gomes, H.S. Bueno, *J. Pet. Sci. Eng.* 199 (2021): p. 108347.
3. Z. Belarbi, J.M. Dominguez Olivo, F. Farelas, M. Singer, D. Young, S. Nešić, *Corrosion* 75 (2019): p. 1246-1254.
4. J. Dominguez Olivo, B. Brown, D. Young, S. Nešić, *Corrosion* 75, 2 (2019): p. 137-139.
5. Y. He, S. Ren, Z. Belarbi, X. Wang, D. Young, M. Singer, "Micellization and Inhibition Efficiency," CORROSION 2021, paper no. 16872 (Houston, TX: AMPP, 2021), p. 1-16.
6. F. Farelas, M. Singer, D. Nugraha, S. Whitehurst, B. Kinsella, "Localized Corrosion in the Presence of Corrosion Inhibitors at High Flow Velocities in CO_2 Environments," CORROSION 2018, paper no. 11269 (Houston, TX: NACE, 2018), p. 1-14.
7. W. Li, B.F.M. Pots, B. Brown, K.E. Kee, S. Nešić, *Corros. Sci.* 110 (2016): p. 35-45.
8. C.S. Brossia, G.A. Cragnolino, *Corrosion* 56 (2000): p. 505-514.
9. G.A. Schmitt, W. Bucken, R. Fanebust, *Corrosion* 48 (1992): p. 431-440.
10. J. Marsh, J.W. Palmer, R.C. Newman, "Evaluation of Inhibitor Performance for Protection against Localized Corrosion," CORROSION 2002, paper no. 02288 (Houston, TX: NACE, 2002).
11. J. Han, "Galvanic Mechanism of Localized Corrosion for Mild Steel in Carbon Dioxide Environments" (Ph.D. diss., Ohio University, 2009).
12. A. Turnbull, D. Coleman, A.J. Griffiths, P.E. Francis, L. Orkney, *Corrosion* 59, 3 (2003): p. 250-257.
13. H. Swenson, N.P. Stadie, *Langmuir* 35, 16 (2019): p. 5409-5426.
14. W.D. Callister, D.G. Rethwisch, *Materials Science and Engineering: An Introduction*, Materials Science and Engineering (2007), http://sinnott.mse.ufl.edu/Syllabus_abet_3010_2007_v02.pdf.
15. Y. He, S. Ren, X. Wang, D. Young, M. Singer, Z. Belarbi, M. Mohamed-Saïd, S. Camperos, M.R. Khan, K. Cimatu, *Corrosion* 78 (2022): p. 625-633.
16. H. Mansoori, R. Mirzaee, F. Esmaeilzadeh, A. Vojood, A.S. Dowrani, *Eng. Fail. Anal.* 82 (2017): p. 16-25.
17. A.M. Nor, M.F. Suhor, M.F. Mohamed, M. Singer, S. Nešić, "Corrosion of Carbon Steel in High CO_2 Environment: Flow Effect," CORROSION 2011, paper no. 11242 (Houston, TX: NACE, 2011).
18. M.A. Pletnev, *Int. J. Corros. Scale Inhib.* 9 (2020): p. 842-866.
19. V.J. Drazic, D.M. Drazic, "Influence of the Metal Dissolution Rate on the Anion and Inhibitor Adsorption," in 7th Eur. Symp. Corros. Inhib. (1990).
20. X. Zhang, F. Wang, Y. He, Y. Du, *Corros. Sci.* 43 (2001): p. 1417-1431.
21. W.J. Lorenz, F. Mansfeld, *Electrochim. Acta* 31 (1986): p. 467-476.
22. ASTM G102-89, "Standard Practice for Calculation of Corrosion Rates and Related Information from Electrochemical Measurements" (West Conshohocken, PA: ASTM International, 2015), p. 1-7.
23. S. Papavinasam, "Evaluation and Selection of Corrosion Inhibitors," in *Uhlig's Corrosion Handbook,* 3rd ed. (Hoboken, NJ: Wiley, 2011), p. 1121-1127.
24. E. McCafferty, *Thermodynamics of Corrosion: Pourbaix Diagrams. In: Introduction to Corrosion Science* (New York, NY: Springer, 2010), http://link.springer.com/10.1007/b97510.
25. R.C. Souza, B.A.F. Santos, M.C. Gonçalves, E.P. Mendes Júnior, T.A. Simões, J.R. Oliveira, G.L. Vaz, L. Caldeira, J.A.C.P. Gomes, A.H. Bueno, *J. Pet. Sci. Eng.* 180 (2019): p. 78-88.
26. A.A. Al-Asadi, "Iron Carbide Development and Its Effect on Inhibitor Performance" (Master's thesis diss., Ohio University, 2014).
27. E. Gulbrandsen, S. Nešić, A. Stangeland, T. Burchardt, *Corrosion* (1998): p. 1-13.
28. K. Kowata, K. Takahashi, "Interaction of Corrosion Inhibitors With Corroded Steel Surface," CORROSION 96, paper no. 96219 (Houston, TX: NACE, 1996).
29. S. Nešić, W. Wilhelmsen, S. Skjerve, S.M. Hesjevik, "Testing of Inhibitors for CO_2 Corrosion Using the Electrochemical Techniques," in Proc. 8th Eur. Symp. Corros. Inhib. (8 SEIC) (1995), p. 1163-1192.